Temporal coherence in mirrorless optical parametric oscillators

Gustav Strömqvist, Valdas Pasiskevicius, Carlota Canalias, Pierre Aschieri, Antonio Picozzi, Carlos Montes

Temporal coherence in mirrorless optical parametric oscillators

Gustav Strömqvist,[1,*] Valdas Pasiskevicius,[1] Carlota Canalias,[1] Pierre Aschieri,[2] Antonio Picozzi,[3] and Carlos Montes[2]

[1]*Department of Applied Physics, Royal Institute of Technology (KTH), Roslagstullsbacken 21, 10691 Stockholm, Sweden*
[2]*LPMC-CNRS, Université de Nice-Sophia Antipolis, Parc Valrose, F-06108 Nice, France*
[3]*Institut Carnot de Bourgogne, F-21078 Dijon Cedex, France*
**Corresponding author: gs@laserphysics.kth.se*

Received November 28, 2011; revised February 8, 2012; accepted February 16, 2012; posted February 16, 2012 (Doc. ID 159036); published May 9, 2012

One of the unique features of mirrorless optical parametric oscillators based on counterpropagating three-wave interactions is the narrow spectral width of the wave generated in the backward direction. In this work, we investigate experimentally and numerically the influence that a strong phase modulation in the pump has on the spectral bandwidths of the parametric waves and on the efficiency of the nonlinear interaction. The effects of group-velocity mismatch and group-velocity dispersion are elucidated. In particular, it is shown that the substantial increase in temporal coherence of the backward-generated wave can be obtained even for pumping with a temporally incoherent pump. A configuration of a mirrorless optical parametric oscillator is proposed where this gain in spectral coherence is maximized without a penalty in conversion efficiency by employing group-velocity matching of the pump and the forward-generated parametric wave.

OCIS codes: 030.1640, 190.4410, 190.4970, 230.4320.

1. INTRODUCTION

Nonlinear parametric interactions where the phase-matched signal and idler waves are generated in opposite directions establish a distributed feedback mechanism, which enables optical parametric oscillation without the need of external mirrors or surface coatings. A device employing this mechanism, the mirrorless optical parametric oscillator (MOPO), was theoretically suggested in 1966 [1] and experimentally realized 40 years later [2] by using periodically-poled $KTiOPO_4$ (PPKTP) with sub-μm periodicity as a quasi-phase-matched (QPM) nonlinear medium. This short periodicity translates into a large QPM grating vector that can compensate for the large momentum mismatch between the counterpropagating waves through QPM of first order. PPKTP crystals with similar periodicities have also been used for the construction of electrically controlled Bragg reflectors through third-order QPM [3] and for backward second-harmonic generation through QPM of sixth and seventh order in waveguides [4] and in bulk [5]. One of the remarkable properties of the MOPO is the strong asymmetry in spectral bandwidth between the signal and the idler pulses: the bandwidth of the forward signal is comparable to the pump bandwidth, whereas that of the backward idler is typically one to two orders of magnitude narrower [6]. It has recently been demonstrated, both experimentally and numerically, that this spectral asymmetry occurs when the pump wave exhibits deterministic phase modulation. In accordance with the convection-induced phase-locking mechanism [7–11], the phase modulation in the pump is coherently transferred to the forward parametric wave, while the backward wave retains a narrow bandwidth and high coherence [12]. This mechanism has previously been verified in a MOPO pumped with relatively narrowband (1.2 THz) linearly chirped pump pulses.

In this work, we experimentally and numerically investigate how the spectral extent and the temporal coherence of the pump, along with the dispersive properties of the nonlinear medium, affect the conversion efficiency and the spectra of the parametric waves generated in a MOPO. The influence of the pump bandwidth on the MOPO operation is experimentally studied by pumping a PPKTP crystal with linearly-chirped pulses of bandwidths up to 4 THz, showing that a broader pump spectrum decreases the conversion efficiency and predominantly broadens the spectrum of the forward parametric wave. The MOPO dynamics is numerically simulated with a new numerical scheme that solves the coupled wave equations in the counterpropagating configuration in the presence of group-velocity dispersion (GVD) by combining the trajectories method for the nonlinear three-wave interaction and fast Fourier transformation (FFT) to account for the GVD effects. We numerically model MOPO operation with linearly chirped pump pulses and quantify the decrease in conversion efficiency for an increasing spectral width. New pumping configurations are also studied, showing that a MOPO may operate even when the pump is incoherent with a phase modulation that varies randomly throughout the pulse. Regardless if the phase modulation in the pump is deterministic or stochastic, the backward parametric wave always has a bandwidth that is narrow compared to that of the forward wave. This effect is especially pronounced if the pump wavelength and the modulation period of the nonlinear medium are chosen so that the group velocities of the pump and the forward wave are exactly matched. Furthermore, with matched group velocities, the MOPO conversion efficiency becomes rather insensitive to the spectral quality of the pump.

This paper is organized as follows: In Section 2., we summarize the MOPO characteristics and emphasize the factors that determine the phase modulation in the parametric waves. The experimental demonstrations of MOPO operation are described in Section 3. and the nonlinear three-wave interaction is simulated numerically in Section 4., where linearly chirped pump pulses are treated in Subsection 4.A. and pump pulses with stochastic phase modulation are used in Subsection 4.B. Finally, we present a summary in Section 5.

2. MOPO PRINCIPLES

In a MOPO, the pump wave is down-converted into forward-propagating and backward-propagating parametric waves, in accordance with energy conservation,

$$\omega_p = \omega_f + \omega_b, \tag{1}$$

and counterpropagating quasi-phase-matching,

$$k_p - k_f + k_b = K_G, \tag{2}$$

where $j = p, f, b$ denote the pump, the forward and the backward parametric waves, respectively. $K_G = 2\pi/\Lambda$ is the grating vector given by Λ, the modulation period of the second-order nonlinear coefficient. The choices of pump wavelength and grating periodicity determine which of the forward and the backward waves that carries the most energy, i.e. which is the signal and which is the idler.

When the crystal is pumped above threshold, the counterpropagating parametric waves automatically establish a distributed-feedback mechanism and thereby optical parametric oscillation without a cavity. The pump intensity required to reach threshold for MOPO operation, $I_{p,\mathrm{th}}$, can be estimated from the plane-wave monochromatic model [13] as

$$I_{p,\mathrm{th}} = \frac{c\varepsilon_0 n_p n_f n_b \lambda_f \lambda_b}{2L^2 d_{\mathrm{eff}}^2}, \tag{3}$$

where c is the speed of light in vacuum, ε_0 is the permittivity of free space, n_j are the refractive indices, λ_j are the backward and forward wavelengths, L is the crystal length and d_{eff} is the effective quadratic nonlinearity. The conversion efficiency is zero at the threshold, but increases rapidly with the pump intensity and reaches almost 80% at two times the threshold value. However, for a pulsed pump, the nonlinear process becomes less efficient and the conversion efficiency must be calculated with numerical methods.

By differentiating Eqs. (1) and (2) while keeping the grating periodicity constant, the rate of change of the frequencies of the parametric waves with respect to the pump frequency can be expressed as functions of the group velocities, $v_{g,j}$ $(j = p, f, b)$, of the three waves [2],

$$\frac{\partial\omega_f}{\partial\omega_p} = \frac{v_{g,f}(v_{g,p} + v_{g,b})}{v_{g,p}(v_{g,f} + v_{g,b})} \equiv 1 + \varepsilon_1, \tag{4}$$

$$\frac{\partial\omega_b}{\partial\omega_p} = \frac{v_{g,b}(v_{g,p} - v_{g,f})}{v_{g,p}(v_{g,f} + v_{g,b})} \equiv -\varepsilon_1. \tag{5}$$

The plus signs in the denominators and in the numerator for the forward wave originate from the counterpropagating geometry. A dimensionless parameter, ε_1, is introduced as a measure of the group-velocity difference between the forward wave and the pump. In wavelength regions where the material is transparent, the group velocity is normally a slowly varying function of the frequency, implying that $|\varepsilon_1| \ll 1$ and that the derivative is close to unity for the forward wave [Eq. (4)] and close to zero for the backward wave [Eq. (5)]. The frequency of the forward wave hence follows the pump as the pump tunes, whereas that of the backward wave stays almost constant. As a numerical example, using a PPKTP crystal with $\Lambda = 800$ nm, $\varepsilon_1 \simeq 0.01$ for a broad range of pump wavelengths in the near-infrared. The very different tuning rates imply that there is an asymmetry in bandwidth between the parametric waves when a broadband pump is used, since all frequencies present in the pump generate almost the same backward frequency. Equivalently, the bandwidth asymmetry can be related to the phase modulation present in the parametric waves, which is transferred from the pump to the forward and backward waves at the same rates as $\partial\omega_f/\partial\omega_p$ and $\partial\omega_b/\partial\omega_p$, thereby being much stronger in the forward wave [12].

If the QPM period, Λ, and the pump frequency, ω_p, are chosen in such a way that the group velocities of the pump and the forward wave are equal, then $\varepsilon_1 = 0$ and from Eq. (5) there is no phase modulation in the backward wave. This is however an approximation, since any pulsed pump contains a continuum of frequencies, which all have slightly different values of ε_1 due to group-velocity dispersion. For a frequency $\omega_p' = \omega_p + \delta\omega_p$ within the pump bandwidth, approximate expressions for the tunabilities at the quasi-phase-matched frequencies ω_j' $(j = f, b)$ are obtained by expanding the equations in Taylor series around $\delta\omega_p = 0$,

$$\frac{\partial\omega_f'}{\partial\omega_p} \simeq \frac{\partial\omega_f}{\partial\omega_p} + \frac{\partial^2\omega_f}{\partial\omega_p^2}\delta\omega_p \equiv 1 + \varepsilon_1 + \varepsilon_2\delta\omega_p, \tag{6}$$

$$\frac{\partial\omega_b'}{\partial\omega_p} \simeq \frac{\partial\omega_b}{\partial\omega_p} + \frac{\partial^2\omega_b}{\partial\omega_p^2}\delta\omega_p \equiv -\varepsilon_1 - \varepsilon_2\delta\omega_p. \tag{7}$$

The second derivatives can be expressed in the group velocities, $v_{g,j}$, and the GVD coefficients, $\beta_{2,j} \equiv (\partial^2 k/\partial\omega^2)_j$, $(j = p, f, b)$ as

$$\begin{aligned}\varepsilon_2 \equiv \frac{\partial^2\omega_f}{\partial\omega_p^2} &= -\frac{\partial^2\omega_b}{\partial\omega_p^2} \\ &= -\frac{v_{g,f}v_{g,b}}{v_{g,f} + v_{g,b}}\left[\beta_{2,f}\left(\frac{\partial\omega_f}{\partial\omega_p}\right)^2 - \beta_{2,p} - \beta_{2,b}\left(\frac{\partial\omega_b}{\partial\omega_p}\right)^2\right].\end{aligned} \tag{8}$$

Equations (6) and (7) quantify how the rate at which the phase modulation is transferred from the pump to the parametric waves varies with the pump bandwidth. Since $|\partial\omega_f/\partial\omega_p| \gg |\partial\omega_b/\partial\omega_p|$, the relative correction introduced by the GVD-related term $\pm\varepsilon_2\delta\omega_p$ given by Eq. (8) is much stronger for the backward wave. Even with a pump bandwidth exceeding several tens of THz, this correction always has a

negligible contribution to the forward-wave spectrum. On the other hand, when $\varepsilon_1 = 0$, the spectral width due to residual phase modulation present in the backward-generated wave will be proportional to the difference in GVD coefficients between the forward wave and the pump, $\beta_{2,f} - \beta_{2,p}$, and also proportional to the pump bandwidth.

The spectral bandwidths of the parametric waves depend on both the amount of phase modulation present in them and on the temporal shapes of the pulses. Phase modulation in the pump gives rise to a temporal frequency shift, $d\omega_p/dt$, which is transferred to the parametric waves by multiplication of $1 + \varepsilon_1$ for the forward wave and $-\varepsilon_1$ for the backward wave. The temporal shape of the pulses sets a lower limit on the bandwidth through the width of its Fourier transform, which scales inversely to its temporal length, τ_p. In the case when the pump bandwidth is strongly dominated by phase modulation, i.e. $|d\omega_p/dt| \gg \tau_p^{-2}$, this property is always inherited by the forward wave. Depending on the value of $|\varepsilon_1|$ and the spectral and temporal properties of the pump, the backward-wave bandwidth can be dominated either by phase modulation or by its temporal duration.

3. EXPERIMENTAL RESULTS

In order to investigate the influence that the phase modulation in the pump has on the spectral properties of the parametric waves generated in a MOPO, we used two pumping configurations, where in both cases the temporal pulse lengths were approximately the same, but the linear chirp rates differed substantially. The pump pulses were derived from a Ti:Sapphire regenerative chirped-pulse amplifier system where the spectral width and the chirp rate of the pulses were adjusted by employing two different sets of stretcher-compressor gratings. Spectral filtering was applied in the stretcher and the output pulse length, measured with autocorrelation, was adjusted by adding an appropriate amount of negative group-delay dispersion in the compressor stage. A 6.5-mm-long PPKTP crystal with the periodicity of $\Lambda = 800$ nm was used as the nonlinear medium, engineered for a quasi-phase-matched interaction between the pump, a near-infrared forward signal, and a backward idler in the mid-infrared. The fabrication details of the crystal are described in [3] and [5].

The pump beam propagated along the x direction of the PPKTP and was loosely focused inside the crystal to a $1/e^2$ intensity radius of 110 μm. A partially transmittive mirror, transparent for the pump and reflective for the idler, was placed in front of the crystal to direct the generated idler beam

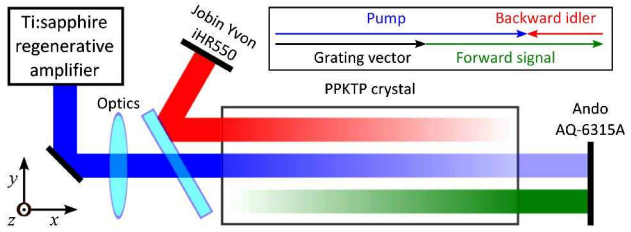

Fig. 1. (Color online) The pump beam is focused inside the PPKTP crystal, generating a signal in the forward direction and an idler in the backward direction, as illustrated in the phase-matching diagram. The parametric beams overlap the pump beam, but have been displaced vertically in the figure. All beams are polarized in the z direction.

into a spectrometer (Jobin Yvon iHR 550). The spectra of the near-infrared pump and signal were measured with a fiber-coupled spectrometer (Ando AQ-6315A) that was placed after the crystal. A schematic sketch of the setup is found in Fig. 1. The pump was linearly polarized along the z direction of the PPKTP and generated z-polarized parametric waves through the largest nonlinear tensor component, d_{33}.

In the first pumping configuration, the pump pulses had a central wavelength of 814.5 nm, a full-width at half-maximum (FWHM) spectral width of 1.1 THz and a FWHM temporal length of 66 ps, giving the pulses an approximately linear frequency chirp of $d\omega_p/dt \simeq -0.10$ ps^2. With this pump, MOPO threshold was reached at the intensity of 1.4 GW/cm^2, which can be compared to 0.8 GW/cm^2 as calculated from Eq. (3) for a monochromatic pump with $d_{\text{eff}} = 9$ pm/V. The input pump and the depleted pump spectra at 1.5 times the MOPO threshold for this narrowband pump are shown in the left panel of Fig. 2(a) by solid and dotted lines, respectively. Note that the spectra, due to the linear chirp, reflect the temporal evolution of the pump depletion. The corresponding signal and idler spectra are displayed in the left panels of Fig. 2(b) and Fig. 2(c), showing a signal generated around 1126.3 nm (FWHM 320 GHz) and an idler around 2952.0 nm (FWHM 27 GHz). The signal and idler peaks correspond to maximum conversion at the pump wavelength of 815.2 nm. By comparing the input and output pump spectra, the average pump depletion at this intensity is estimated to be 28%.

The other pumping configuration was used to test the possibility of MOPO operation with pulses of broad spectral width and strong phase modulation. The pump was tuned to a central wavelength of 858.0 nm and the FWHM bandwidth was increased to 4.0 THz. After the compressor, the FWHM

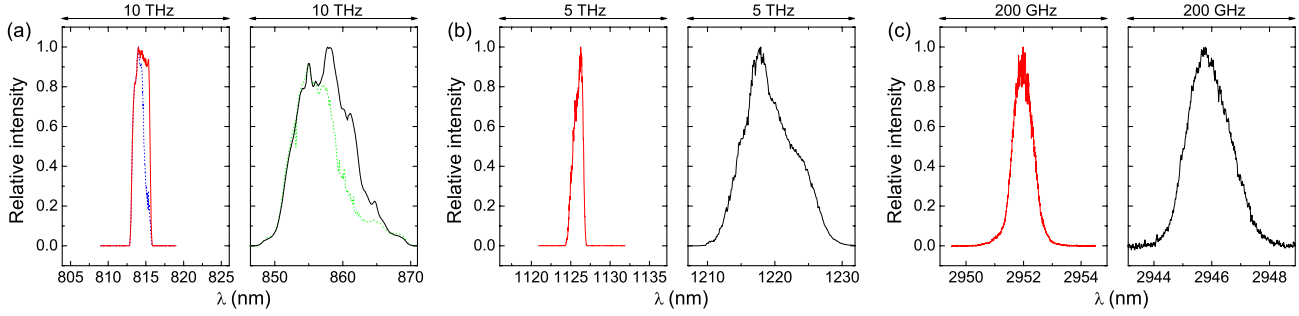

Fig. 2. (Color online) Experimental spectra corresponding to the narrowband pump at 814.5 nm (left panel) and the broadband pump at 858.0 nm (right panel). (a) Undepleted (solid line) and depleted (dotted line) pump spectra with initial FWHM spectral widths of $\Delta\nu_p = 1.08$ THz and $\Delta\nu_p = 3.98$ THz. (b) Forward signals around 1126.3 nm ($\Delta\nu_f = 320$ GHz) and 1217.9 nm ($\Delta\nu_f = 1.62$ THz). (c) Backward idlers around 2952.0 nm ($\Delta\nu_b = 27$ GHz) and 2945.7 nm ($\Delta\nu_b = 59$ GHz).

temporal length was 50 ps and the chirp rate was -0.49 rad/ps^2. The MOPO reached threshold at the intensity of 1.5 GW/cm^2, which is slightly higher than for the narrowband pump pulse. The spectra of the pump, the signal, and the idler measured at 1.7 times the threshold intensity are shown in the right panels of Fig. 2(a), Fig. 2(b) and Fig. 2(c). A comparison of the undepleted (solid line) and depleted pump (dotted line) reveals that after an initial delay required for establishing the distributed feedback, the pump power is very efficiently depleted in the MOPO. The MOPO reaches the maximum efficiency at the moment when the pump wavelength is 861.7 nm, corresponding to the wavelengths of the signal peak at 1217.9 nm (FWHM 1.6 THz) and the idler peak at 2945.7 nm (FWHM 59 GHz). The average pump depletion is estimated to be 21%, which is less than the 28% depletion of the narrowband pump at the lower relative intensity of 1.5 times threshold. The experiments show that a MOPO pumped with a broadband phase-modulated pump has approximately the same threshold as in the case of narrowband pumping. However, the stronger phase modulation somewhat reduces the conversion efficiency. In accordance with the reasoning in Section 2, the increased pump phase modulation is mostly transferred to the forward signal wave.

By comparing the spectra of the parametric waves generated by the two different pump pulses, several MOPO properties can be verified. For our PPKTP crystal with a QPM period of 800 nm, the calculated tunabilities, Eqs. (4) and (5), are $\partial\omega_f/\partial\omega_p = 1.01 \pm 0.002$ and $\partial\omega_b/\partial\omega_p = -0.01\mp 0.002$ for all pump wavelengths between 780 nm and 950 nm. By changing pumping configuration, the position of maximum conversion is here shifted from 861.7 nm to 815.2 nm, which is a frequency shift of 19.8 THz. This causes the signal to shift by 20.0 THz, whereas the shift in the idler is only −0.2 THz. Thus the signal tunes slightly faster than the pump, whereas the frequency of the idler changes only slowly in the opposite direction, which is in good agreement with calculations. Note that the idler bandwidth is narrow compared to that of the signal, which in both pumping configurations is very close to the width of the depleted part of the pump spectrum.

The temporal duration of the parametric waves can be estimated from the measured spectra and the linear chirp rates of the pump and the forward signal. It has been experimentally verified that a MOPO pumped with a linearly chirped pump gives rise to a linearly chirped forward wave with a similar chirp rate as the pump [12]. A linear chirp is a one-to-one frequency-to-time mapping, meaning that a spectral measurement contains temporal information about the pulses if the chirp rate is known. In both pumping configurations, the FWHM pulse lengths of the parametric waves are then approximately 20 ps. Assuming Gaussian pulse shapes, this pulse length corresponds to a transform-limited bandwidth of 22 GHz. The bandwidth of the narrower idler, measured to 27 GHz, is very close to this value, meaning that its spectral width is predominantly determined by its temporal shape. On the other hand, the pump with large phase modulation generated a backward-propagating idler with a FWHM spectral width of 59 GHz, indicating that the remnant phase modulation contributes appreciably to the idler spectrum. This effect is expected to be more pronounced with a further increased phase modulation in the pump, unless the group velocities of the pump and the forward propagating wave are perfectly matched, as will be shown below.

4. NUMERICAL MODEL

Numerical simulations of the nonlinear three-wave interactions in a MOPO were performed by solving the coupled wave equations in the slowly-varying envelope approximation. The field amplitudes, $\mathbf{A_j}$ ($\mathbf{j} = \mathbf{p}, \mathbf{f}, \mathbf{b}$), of the pump and the parametric waves evolve in accordance with the following set of coupled equations:

$$\begin{aligned}(\partial_t + v_{g,p}\partial_x + \gamma_p + i\beta_p\partial_{tt})\mathbf{A_p} &= -\sigma_p\mathbf{A_f}\mathbf{A_b}\\ (\partial_t + v_{g,f}\partial_x + \gamma_f + i\beta_f\partial_{tt})\mathbf{A_f} &= \sigma_f\mathbf{A_p}\mathbf{A_b^*}\\ (\partial_t - v_{g,b}\partial_x + \gamma_b + i\beta_b\partial_{tt})\mathbf{A_b} &= \sigma_b\mathbf{A_p}\mathbf{A_f^*},\end{aligned} \tag{9}$$

where $\sigma_j = 2\pi d_{\mathrm{eff}} v_{g,j}/\lambda_j n_j$ are the nonlinear coupling coefficients, d_{eff} is the effective quadratic nonlinearity, γ_j and $\beta_j \equiv v_{g,j}\beta_{2,j}/2$ are the damping and dispersion coefficients. The input parameters in the model are the properties of the nonlinear medium and the pump amplitude at the input crystal face, $\mathbf{A_p}(x = 0, t)$, generating outputs of $\mathbf{A_p}(x = L, t)$, $\mathbf{A_f}(x = L, t)$, and $\mathbf{A_b}(x = 0, t)$, where $x = 0$ and $x = L$ denote the positions of the crystal input and output faces with respect to the pump beam. In all simulations, the nonlinear medium is a PPKTP crystal with $L = 6.5$ mm, $d_{\mathrm{eff}} = 9$ pm/V, and dispersion parameters that are calculated from the Sellmeier expansion in [14].

For the numerical treatment of the coupled wave equations for counterpropagating interactions, the standard split-step one-directional integration algorithm, usually employed for copropagating interactions, is not suitable due to the fact that Eq. (9) represents a problem with two simultaneous, but spatially separate, boundary conditions, i.e., the pump and the signal waves are initially given at one end of the crystal, while the idler wave is input from the other end of the crystal. For such problems, there are two main appropriate numerical methods: the shooting or trajectories method and the relaxation method. For the problem at hand, the trajectories method is more convenient, whereby we eventually want to simulate a counterpropagating three-wave mixing process driven by a pump field with a quasi-random phase distribution. The trajectories method with the use of a Runge–Kutta algorithm has been extensively used for the treatment of stimulated Brillouin back-scattering problems [15–16].

The linewidth narrowing experimentally studied in Brillouin lasers [17] has been simulated in a Brillouin fiber-ring laser with the help of this method [18]. In that case, it is the acoustic wave that absorbs the phase fluctuations of the pump and allows the backward Stokes wave to increase its coherence. In order to numerically integrate the nonlinear counterpropagation dynamics in a MOPO in the presence of group-velocity dispersion (GVD), which introduces second-order time derivatives, we have developed a new numerical scheme which combines the trajectories method with fast Fourier transformation (FFT) to account for the GVD effects in the spectral domain. The scheme accurately conserves the number of photons and the Manley–Rowe invariants of Eq. (9). As in the standard split-step approach, the evolution of Eq. (9) is for each time step (typically 1 fs long) first treated by linear propagation of the fields in the Fourier domain,

thereby accounting for the GVD effects and the group-velocity difference between the pump and the copropagating wave. The originality with respect to the standard split-step schemes with multiply repeated FFT and inverse FFT procedures where exponential spectral cutoff filtering is introduced at the edges of the spectrum, is that we here introduce smoothed exponentially decreasing prolongations of the outgoing complex amplitudes (over a length d) in the x-space of the MOPO crystal (of length L) in order to render a periodic problem. Thus the FFT is correctly performed in the extended crystal of length $M = L + 2d$ without arbitrary cutoffs. Then, after inverse FFT, the backward nonlinear interaction with spatially separate boundary conditions is treated by using the trajectories method. Integration over the trajectories in the nonlinear step of the algorithm was performed by using a fourth-order fixed-step Runge–Kutta method. The space-time is discretized in 2^N points with $N = 16$ to 18, which, for instance, when $N = 16$ allows for a total bandwidth of 35 THz with the resolution of 0.5 GHz.

The algorithm is seeded by an appropriate model pump field entering from one side of the nonlinear crystal and homogeneously spatially distributed signal and idler fields with powers corresponding to a half photon per mode and with random phases, representing quantum noise. During the field evolution, we checked that the Manley–Rowe invariants were preserved to the accuracy of better than 10^{-5}, even after numerically evolving Eq. (9) over 6×10^6 time steps. The results obtained with our method were compared with those obtained using a fourth-order finite-difference scheme. For the chirped input pump pulse, where differentiability is ensured, the same quantitative results are obtained with both methods. The latter scheme, however, is not adapted for incoherent pulses.

A. Linearly-Chirped Pump Pulse

MOPO operation in a PPKTP crystal of period $\Lambda = 800$ nm is simulated with a linearly chirped pump pulse with a central wavelength of 861.7 nm. The input pump amplitude is chosen to be Gaussian and given by

$$\mathbf{A_p}(x = 0, t) = \mathbf{A_p^0} \exp[i\phi_p(t - t_0)] \exp\{-2 \ln 2[(t - t_0)/\Delta t_0]^2\}. \tag{10}$$

The spectral and temporal shapes of the pulse are determined by the phase modulation, $\phi_p(t)$, and the FWHM temporal length, Δt_0. With a linear chirp, the phase modulation is quadratic in time, $\phi_p(t) = \alpha_2 t^2$, where the value of the chirp parameter $\alpha_2 = -0.244$ rad/ps^2 is chosen to obtain the chirp rate of $d\omega_p/dt = -0.49$ rad/ps^2. With this chirp, a temporal intensity FWHM of $\Delta t_0 = 52$ ps gives a FWHM spectral width of 4.04 THz. The dispersion parameters in a KTP crystal at the pump and the parametric wavelengths are found in Table 1, having a group-velocity difference that corresponds to $\varepsilon_1 \simeq 9.8 \times 10^{-3}$ that varies throughout the FWHM bandwidth with approximately 2%, as ε_2 corresponds to 5.5×10^{-5}/THz in cyclic frequency.

Table 1. Dispersion Data for z-Polarized Waves in $KTiOPO_4$[a]

	λ_j (nm)	n_j	$v_{g,j}/c$	$\beta_{2,j}$ (ps^2/m)
Pump (p)	861.67	1.8400	0.5269	0.2473
Signal (f)	1217.94	1.8243	0.5372	0.1343
Idler (b)	2945.73	1.7806	0.5334	−0.6413

[a]index of refraction (n_j), group velocity ($v_{g,j}$) and GVD coefficient ($\beta_{2,j} = \partial^2 k/\partial\omega^2$) at wavelengths ($\lambda_j$).

As the pump pulse enters the crystal, a forward signal and a backward idler are generated with similar spectral characteristics as those obtained in the experiments. The pump and the parametric spectra at the pump intensity of 2.34 GW/cm^2 are illustrated in Fig. 3, showing a backward idler with a spectral width of $\Delta\nu_b = 51$ GHz, which is narrow compared to the widths of the pump, $\Delta\nu_p = 4.04$ THz, and the forward signal, $\Delta\nu_f = 1.78$ THz. By integrating the spectra, it is found that the conversion into parametric waves here is $I_f(L)/I_p(0) = 0.036$ for the signal and $I_b(0)/I_p(0) = 0.014$ for the idler. As expected from the convection-induced phase-locking mechanism, the phase modulation in the pump is essentially transferred to the forward signal, while the phase of the backward idler is approximately constant. This is further illustrated in Fig. 4 where the phase distributions of the waves are plotted inside the crystal at the time $t = 141$ ps . Figure 4(a) corresponds to the simulation with the dispersion data in Table 1, showing that the signal phase approximately follows the phase of the pump, whereas the idler phase is only weakly modulated. As a comparison, the phases of a simulation with perfect group-velocity matching between the forward signal and the pump is shown in Fig. 4(b). The same dispersion relation is used, with the change that $v_{g,f} = v_{g,p}$ so that $\varepsilon_1 = 0$. The phase modulation in the pump is then almost completely transferred to the forward signal and the phase of the backward idler is practically constant throughout the crystal.

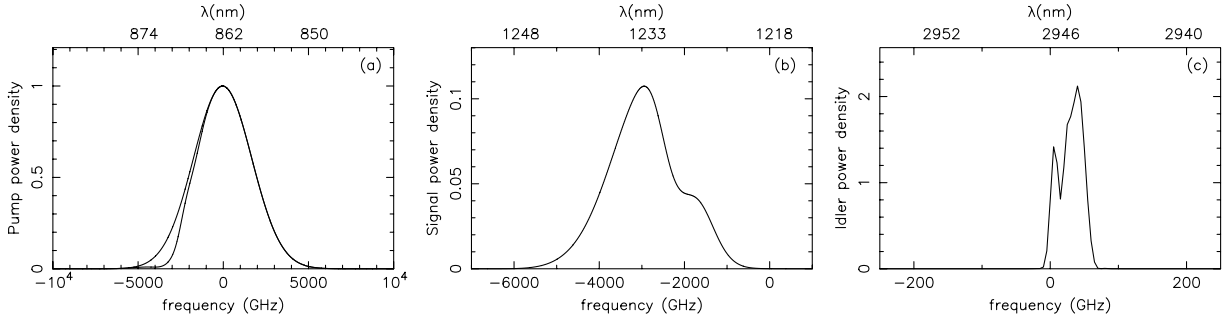

Fig. 3. (a) Undepleted input and depleted output pump spectrum of $\Delta\nu_p = 4.04$ THz, (b) the forward signal spectrum with $\Delta\nu_f = 1.78$ THz, and (c) the backward idler spectrum with $\Delta\nu_b = 51$ GHz.

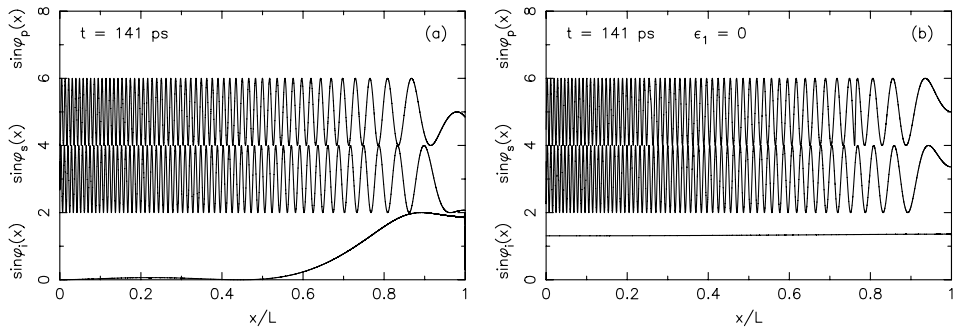

Fig. 4. Phase distributions inside the crystal for the pump, the forward signal (locked to the pump) and the backward idler (invariant) at the time $t = 141$ ps. (a) Describes the experimental conditions, $\varepsilon_1 \simeq 9.8 \times 10^{-3}$ and (b) describes the case of ideal group-velocity matching, $\varepsilon_1 = 0$.

By running simulations with pump pulses of different spectral widths, it is observed that the conversion efficiency decreases as the pump spectrum broadens when the group-velocity difference between the forward wave and the pump is the same as in the experiments and $\varepsilon_1 \simeq 9.8 \times 10^{-3}$. This behavior is due to the nonzero convective velocity $|v_{g,p} - v_{g,f}|$ of the comoving waves, i.e. a finite temporal walk-off, which makes the spectral components in the signal move past those in the pump. On the other hand, for perfect group-velocity matching ($v_{g,f} = v_{g,p}$, $\varepsilon_1 = 0$), there is no temporal walk-off and the conversion efficiency is constant as the pump spectrum broadens, since the pump and the signal move at the same velocity. The pump depletion, $1 - I_p(L)/I_p(0)$, and the conversion efficiencies into signal, $I_f(L)/I_p(0)$, and idler, $I_b(0)/I_p(0)$, were systematically investigated for linearly chirped Gaussian pump pulses where the temporal pulse shape was held constant with a FWHM length of 52 ps and a peak intensity of 2.57 GW/cm^2. The spectral width was controlled by varying the chirp parameter α_2 from 0 to −0.30 rad/ps^2, corresponding to a FWHM bandwidth from the transform limit up to about 5 THz. In Fig. 5, the three lower curves show how the pump depletion and the conversion efficiency into signal and idler decrease as the pump bandwidth increases. Each point on the curves corresponds to a mean value over a set of simulations with random initial phases, i.e. the phase modulation is given by $\phi(t) = \alpha_2 t^2 + \phi_0$, where

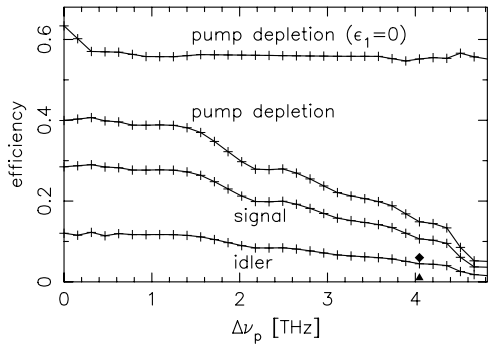

Fig. 5. Pump depletion, $1 - I_p(L)/I_p(0)$, and conversion efficiencies for the signal, $I_f(L)/I_p(0)$, and for the idler, $I_b(0)/I_p(0)$, in the MOPO as function of the pump bandwidth for linearly chirped pulses at the pump intensity of $I_p = 2.57$ GW/cm^2. The three lower curves correspond to the experimental condition, $\varepsilon_1 \simeq 9.8 \times 10^{-3}$, which clearly show a decrease in the efficiency as the pump bandwidth increases. The upper curve shows that the pump depletion is essentially independent of the pump bandwidth when $\varepsilon_1 = 0$. The pump depletion for the stochastic pump at the intensities of 2.57 GW/cm^2 (black triangle) and 3.5 GW/cm^2 (black diamond) are also marked in the graph.

ϕ_0 is a random number. The efficiency is slightly different for each choice of ϕ_0 and the value typically varies within the vertical bar of the plus signs associated to each point. At some points, there is an apparent increase in the efficiency with an increased pump bandwidth, which is due to the limited set of random initial phases ($n = 6$) used for the averaging. However, the main behavior is that a broader pump input spectrum decreases the efficiency of the MOPO process when the group-velocities of the forward wave and the pump are not matched.

The upper curve in Fig. 5 shows the pump depletion when the group velocities of the pump and the forward-propagating wave are matched, $v_{g,f} = v_{g,p}$. This gives a direct comparison between the two cases when $\varepsilon_1 \simeq 9.8 \times 10^{-3}$ and $\varepsilon_1 = 0$ and shows that the nonlinear interactions in a MOPO become more efficient in the case of group-velocity matching ($\varepsilon_1 = 0$). Furthermore, the pump depletion (or the conversion efficiency) then also becomes rather insensitive to the spectral quality of the pump, due to the absence of temporal walk-off.

B. Incoherent Pump Pulse

One question that arises is if a MOPO can operate when it is pumped with incoherent pulses. It is not obvious that such pulses can generate a spectrally narrow backward-propagating parametric wave, which is a characteristic feature of a MOPO. In the conventional copropagating configuration, the generation of a temporally coherent wave from a temporally incoherent pump has been numerically studied for i.e. parametric down-conversion [19] and has been experimentally verified for second-harmonic generation [20]. In order to answer the question in the counterpropagating MOPO configuration, we used a pump pulse with randomly distributed phase variations, characterized by an exponential correlation function,

$$\langle \mathbf{A_p}(x = 0, t' + t)\mathbf{A_p^*}(x = 0, t')\rangle = |\mathbf{A_p}|^2 \exp(-|t|/\tau_c), \quad (11)$$

where $\tau_c = 1/\pi\Delta\nu_p$ is the correlation time. More precisely, we use a numerical scheme to generate a Gaussian spectrum with randomly distributed phases and a small random variation in the amplitude, which simulates a real laser output where the amplitude exhibits small fluctuations over its Gaussian shape. In order to obtain a well-behaved Gaussian input, we impose a Gaussian profile on the Fourier spectrum and the pump amplitude is entered as the inverse Fourier transform. The bandwidth is chosen to be the same as for the linearly chirped pulse

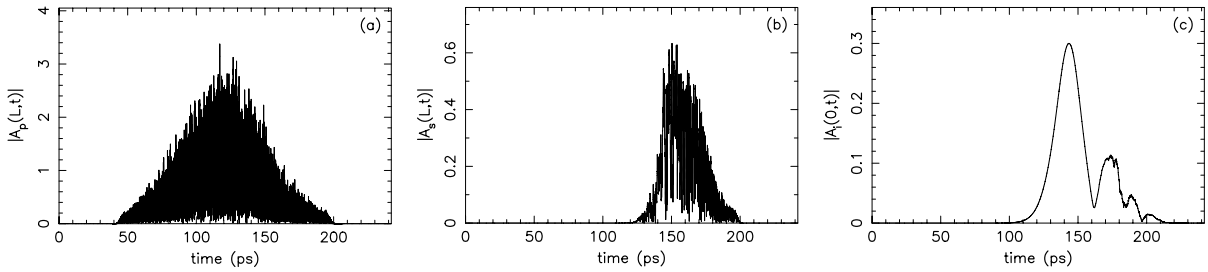

Fig. 6. Temporal evolution of the amplitudes in a MOPO with the interacting wavelengths in Table 1, pumped with pulses of stochastic phase modulation and a bandwidth of $\Delta\nu_p = 4.04$ THz: (a) the forward pump, (b) the forward signal, and (c) the backward idler.

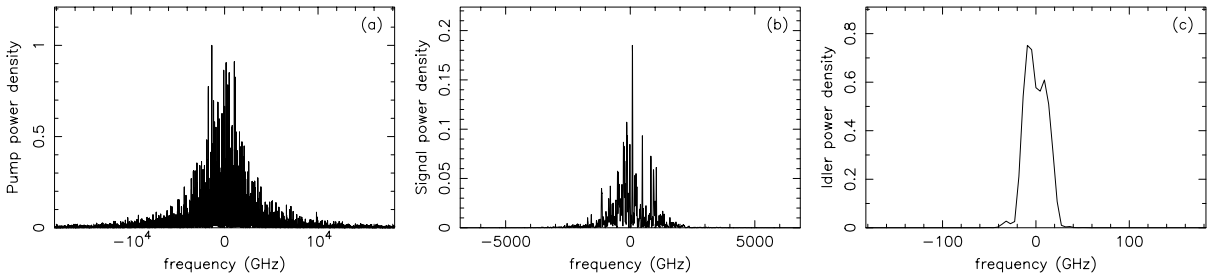

Fig. 7. (a) Incoherent pump spectrum with a bandwidth of $\Delta\nu_p = 4.04$ THz, (b) the signal spectrum with $\Delta\nu_f = 1.42$ THz, and (c) the backward idler spectrum with $\Delta\nu_b = 33$ GHz.

in the previous section, $\Delta\nu_p = 4.04$ THz, and the temporal FWHM pulse duration is 54 ps. With the central wavelengths in Table 1, Fig. 6 and Fig. 7 illustrate the results of a simulation at the pump intensity of $I_p = 3.5$ GW/cm^2.

In Fig. 6, it can be seen that the MOPO starts oscillating after an initial delay of $t - t_0 = 50$ ps and then the parametric waves increase up to relative intensities of $I_f(L)/I_p(0) = 0.0403$ for the signal and $I_b(0)/I_p(0) = 0.0167$ for the idler. Compared to pulses with deterministic phase modulation, stochastic phase fluctuations in the pump have a more detrimental effect on the MOPO conversion efficiency. Even though the pump intensity was increased by 36% to 3.5 GW/cm^2, the pump depletion was only 5.7% compared to 15.7% for a linearly-chirped pump at 2.57 GW/cm^2 with the same bandwidth. For comparison, the pump depletion for a random pump at 2.57 GW/cm^2 and 3.5 GW/cm^2 are marked with data points in Fig. 5.

Figure 7 shows the spectra of the pump, the signal and the idler. Note that the spectrum of the backward idler is narrow, $\Delta\nu_b = 33$ GHz, compared to $\Delta\nu_p = 4.04$ THz for the pump and $\Delta\nu_f = 1.42$ THz for the forward signal. Consequently, the idler spectrum is more than two orders of magnitude narrower than that of the pump, $\Delta\nu_b/\Delta\nu_p \simeq 1/122$. The stochastic phase jumps in the pump are transferred to the signal, thus allowing the counterpropagating idler to evolve toward a highly coherent state. This shows that the convection-induced phase-locking mechanism is efficient for both deterministic phase modulation and random phase fluctuations.

As a result of the phase-locking mechanism, the transfer of phase modulation to the forward wave becomes more efficient when the group velocities of the pump and the forward parametric wave are exactly matched [8]. This was shown in Fig. 4 by the use of an artificial dispersion relation, which also led to an increased pump depletion, as was shown in Fig. 5. For z-polarized waves in PPKTP, matching of the group velocities can be achieved by designing the experiment so that the pump and the forward wave are on different sides of the maximum on the group-velocity curve shown in Fig. 8. However, the combination of exact group-velocity matching and

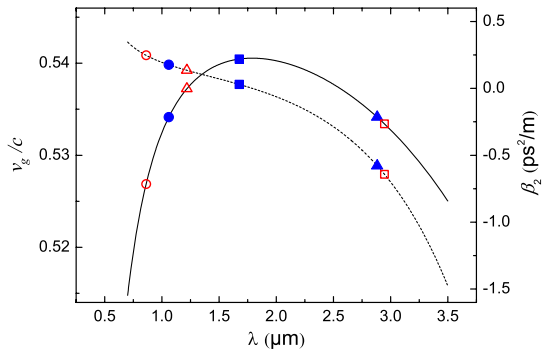

Fig. 8. (Color online) Group velocity (solid line) and group-velocity dispersion (dashed line) for z-polarized waves in $KTiOPO_4$ as function of the wavelength, calculated from the Sellmeier expansion in [14]. The symbols denote the pump (circle), the forward wave (triangle) and the backward wave (square) at the wavelengths in Table 1 (open symbols) and Table 2 (solid symbols).

Table 2. Dispersion Data for z-Polarized Waves in $KTiOPO_4$[a]

	λ_j (nm)	n_j	v_{gj}/c	$\beta_{2,j}$ (ps^2/m)
Pump (p)	1060.00	1.8298	0.5341	0.1752
Signal (b)	1676.46	1.8129	0.5405	0.0290
Idler (f)	2882.66	1.7826	0.5341	−0.5784

[a]index of refraction (n_j), group-velocity (v_{gj}) and GVD coefficient ($\beta_{2,j} = \partial^2 k/\partial\omega^2$) at wavelengths ($\lambda_j$).

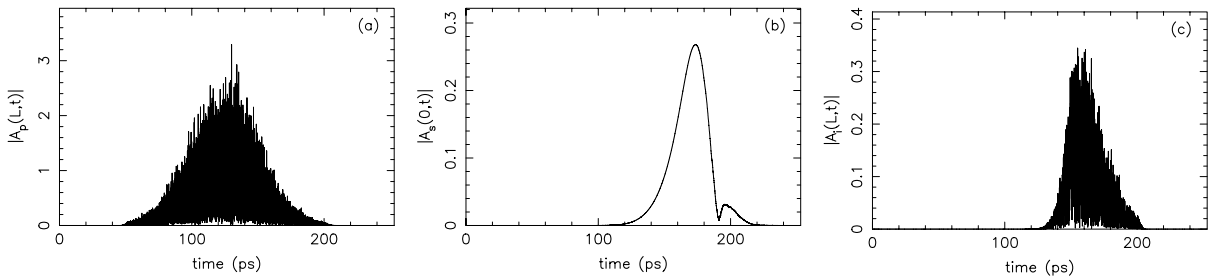

Fig. 9. Temporal evolution of the amplitudes in a MOPO with the interacting wavelengths in Table 2, pumped with pulses of stochastic phase modulation and a bandwidth of $\Delta\nu_p = 23$ THz: (a) the forward pump, (b) the backward signal, and (c) the forward idler.

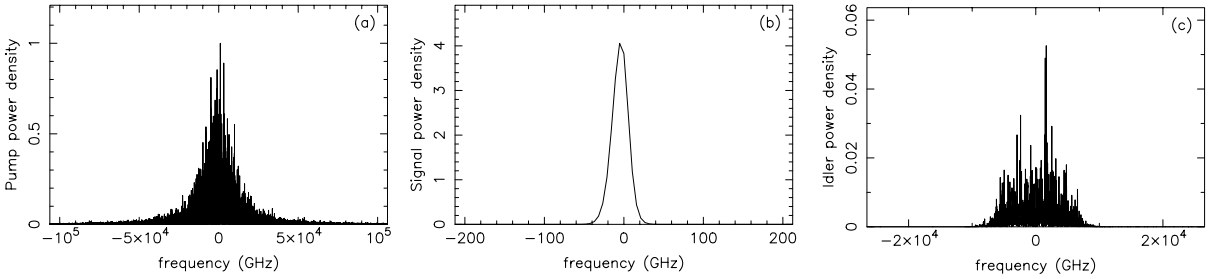

Fig. 10. (a) Incoherent pump spectrum with a bandwidth of $\Delta\nu_p = 23$ THz, (b) the backward signal spectrum with $\Delta\nu_b = 23$ GHz, (c) the forward idler spectrum with $\Delta\nu_f = 10$ THz.

quasi-phase-matching requires either a very short QPM period, which is hard to fabricate, or that the pump wavelength is substantially longer, which increases the MOPO threshold. One example of a set of wavelengths that fulfill group-velocity matching is found in Table 2. For these wavelengths, the forward wave is the idler and the QPM period has to be 456.7 nm. The condition $\varepsilon_1 = 0$ is satisfied for the central pump and idler wavelengths and for the other wavelengths in the pump it must be taken into account that ε_2 corresponds to 3.8×10^{-4}/THz due to the difference in dispersion parameters for the pump and the idler. Around the point of group-velocity matching, the MOPO becomes more efficient and the spectral quality of the pump can be reduced without a large effect on the conversion efficiency. This is illustrated by running a simulation with a stochastic pump with a FWHM temporal length of 50 ps and where the spectral width is increased to 23 THz.

At the pump intensity of 3.5 GW/cm^2, the results are shown in Fig. 9 and Fig. 10. The MOPO starts oscillating after $t - t_0 =$ 60 ps and the conversion efficiencies are $I_b(0)/I_p(0) = 0.025$ for the signal and $I_f(L)/I_p(0) = 0.015$ for the idler. Because of the group-velocity matching, the bandwidth of the backward signal is only 23 GHz. This value is significantly smaller than the bandwidth of backward-wave in Fig. 7(c), even though the pump bandwidth here has been increased by almost a factor of six. In the case of group-velocity matching under the stated operational conditions, the spectral width of the backward-generated wave is reduced by a factor of 1000 compared to the width of the input pump spectrum. The random phase fluctuations in the pump are efficiently transferred to the forward idler, which obtains a spectral width of 10 THz.

For the experimental verification of MOPO operation with an incoherent pump, a laser source is required that generates sub-ns pulses of energies around 100 μJ, at the same time as the pulses are incoherent. Good candidates for such a pump source are figure-eight fiber lasers operating in noiselike pulse mode with pulse lengths around 1 ns [21], which could be amplified to the required energies in fiber amplifiers.

5. SUMMARY

In summary, we have experimentally realized mirrorless optical parametric oscillation in a PPKTP crystal by using linearly chirped pump pulses with bandwidths of up to 4 THz. It has been shown that the spectral bandwidth of the backward-generated wave is about two orders of magnitude narrower than that of the pump. In a general situation, the gain in temporal coherence of the backward-generated wave is limited by the group-velocity mismatch between the pump and the forward-generated wave. This mismatch also limits the conversion efficiency in the MOPO. Numerically, we proved that the same conclusions are valid regardless of the nature of the phase modulation present in the pump wave by simulating operation of a MOPO pumped by waves containing stochastic phase distributions. Moreover, we propose a generic MOPO configuration where the group-velocity matching can be achieved, thereby maximizing the gain in temporal coherence in the backward-propagating wave and making the efficiency of the device insensitive to the nature of the phase modulation present in the pump wave. This opens up an intriguing possibility for narrowband generation in MOPOs pumped with incoherent beams, e.g., derived from several lasers. Albeit the realization of such a MOPO requires QPM crystals which are slightly beyond the state-of-the-art of the current poling technology, the requirements are not unrealistic and can be met with the continuing development in fabrication techniques of submicrometer-periodicity nonlinear crystals. Improved fabrication techniques could also lead to the possibility of poling longer crystals. As the threshold intensity scales inversely to the square of the length of the structured region, an increase of this length from 6.5 mm to 18 mm results

in a threshold intensity around 100 MW/cm^2, which is comparable to that in conventional copropagating PPKTP OPOs.

ACKNOWLEDGMENTS

The authors acknowledge the GDR PhoNoMi2 no. 3073 of the CNRS (Centre National de la Recherche Scientifique) devoted to Nonlinear Photonics in Microstructured Materials, and financial support from the Swedish Research Council (VR) and the Göran Gustafsson Foundation.

REFERENCES

1. S. E. Harris, "Proposed backward wave oscillation in the infrared," Appl. Phys. Lett. **9**, 114–116 (1966).
2. C. Canalias and V. Pasiskevicius, "Mirrorless optical parametric oscillator," Nat. Photon.. **1**, 459–462 (2007).
3. C. Canalias, V. Pasiskevicius, R. Clemens, and F. Laurell, "Submicron periodically poled flux-grown $KTiOPO_4$," Appl. Phys. Lett. **82**, 4233–4236 (2003).
4. M. Xiaodong, I. B. Zotova, Y. J. Ding, and W. P. Risk, "Backward second-harmonic generation in submicron-period ion-exchanged $KTiOPO_4$ waveguide," Opt. Commun. **181**, 153–159 (2000).
5. C. Canalias, V. Pasiskevicius, M. Fokine, and F. Laurell, "Backward quasi-phase matched second harmonic generation in submicrometer periodically poled flux-grown $KTiOPO_4$," Appl. Phys. Lett. **86**, 181105 (2005).
6. V. Pasiskevicius, C. Canalias, G. Strömqvist, and F. Laurell, "Mirrorless OPO: first steps towards unlocking the potential of counter-propagating three-wave interactions" (invited), Proc. SPIE **6875**, 687508 (2008).
7. A. Picozzi and M. Haelterman, "Parametric three-wave soliton generated from incoherent light," Phys. Rev. Lett. **86**, 2010–2013 (2001).
8. A. Picozzi, C. Montes, and M. Haelterman, "Coherence properties of the parametric three-wave interaction driven from an incoherent pump," Phys. Rev. E **66**, 056605 (2002).
9. C. Montes, A. Picozzi, and K. Gallo, "Ultra-coherent output from an incoherent cw-pumped singly resonant optical parametric oscillator," Opt. Commun. **237**, 437–449 (2004).
10. A. Picozzi and P. Aschieri, "Influence of dispersion on the resonant interaction between three incoherent waves," Phys. Rev. E **72**, 046606 (2005).
11. C. Montes, W. Grundkötter, H. Suche, and W. Sohler, "Coherent signal from incoherently cw-pumped singly resonant Ti:LiNbO3 integrated optical parametric oscillators," J. Opt. Soc. Am. B **24**, 2796–2806 (2007).
12. G. Strömqvist, V. Pasiskevicius, C. Canalias, and C. Montes, "Coherent phase-modulation transfer in counterpropagating parametric down-conversion," Phys. Rev. A **84**, 023825 (2011).
13. Y. J. Ding and J. B. Khurgin, "Backward optical parametric oscillators and amplifiers," IEEE J. Quantum Electron. **32**, 1574–1582 (1996).
14. K. Kato and E. Takaoka, "Sellmeier and thermo-optic dispersion formulas for KTP," Appl. Opt. Suppl. **41**, 5040 (2002).
15. C. Montes, A. Mikhailov, A. Picozzi, and F. Ginovart, "Dissipative three-wave structures in stimulated backscattering. I. A subluminous solitary attractor," Phys. Rev. E **55**, 1086–1091 (1997).
16. C. Montes, A. Picozzi, and D. Bahloul, "Dissipative three-wave structures in stimulated backscattering. II. Superluminous and subluminous solitons," Phys. Rev. E **55**, 1092–1106 (1997).
17. S. P. Smith, F. Zarinetchi, and S. Ezekiel, "Narrow-linewidth stimulated Brillouin fiber laser and applications," Opt. Lett. **16**, 393–395 (1991).
18. E. Picholle, C. Montes, C. Leycuras, O. Legrand, and J. Botineau, "Observation of dissipative superluminous solitons in a Brillouin fiber ring laser," Phys. Rev. Lett. **66**, 1454–1457 (1991).
19. A. Piskarskas, V. Pyragaite, and A. Stabinis, "Generation of coherent waves by frequency up-conversion and down-conversion of incoherent light," Phys. Rev. A **82**, 053817 (2010).
20. A. Stabinis, V. Pyragaite, G. Tamošauskas, and A. Piskarskas, "Spectrum of second-harmonic radiation generated from incoherent light," Phys. Rev. A **84**, 043813 (2011).
21. K. Özgören, B. Öktem, S. Yilmaz, F. Ö. Ilday, and Koray Eken, "83 W, 3.1 MHz, square-shaped, 1 ns-pulsed all-fiber-integrated laser for micromachining," Opt. Express **18**, 17647–17652 (2011).